

Double-loop microtrap for ultracold atoms

Bin Jian and William Arie van Wijngaarden*

Physics Department, Petrie Building, York University, 4700 Keele Street, Toronto, Ontario M3J 1P3, Canada

*Corresponding author: wlaser@yorku.ca

Received October 22, 2012; revised December 4, 2012; accepted December 4, 2012;
posted December 5, 2012 (Doc. ID 178170); published January 3, 2013

A microtrap consisting of two concentric circular wire loops having radii of 300 and 660 μm , respectively, is demonstrated. The three-dimensional trap has a maximum depth of more than 1 mK, and the trap center position as measured below the atom chip surface can be adjusted by applying a small-bias magnetic field. More than 10^5 ^{87}Rb atoms were transferred into the microtrap from a magneto-optical trap and remained trapped for several hundred milliseconds, which is limited by the background pressure. The loading of a linear array of three microtraps is also demonstrated. The trap dimensions are readily scaled to micrometer size, which is of interest for creating a one- and two-dimensional array of neutral atom traps on a single atom chip. © 2013 Optical Society of America

OCIS codes: 020.0020, 020.3320.

1. INTRODUCTION

Significant progress has been made during the last decade in the development of magnetic microtraps [1–3]. These traps require one or even two orders of magnitude less current to generate a magnetic field sufficient to trap atoms than is required using macroscopic coils. Moreover, microtraps generate larger magnetic-field gradients and curvatures that can be used to create dense clouds of ultracold atoms required to achieve Bose–Einstein condensation (BEC) [4–7] or degenerate Fermi gases [8]. An important advantage of microtraps is that BECs can be generated in times of seconds rather than nearly 1 min using macroscopic coils [9]. Microtraps facilitate the manipulation of ultracold atoms in a number of novel applications including surface microscopy [10,11], atom Michelson interferometers [12], manipulation of matter waves [13], studies of atom-field coupling between BECs and an optical cavity [14], precision force sensing, [15] and quantum-information processing [16,17].

This work demonstrates a magnetic microtrap that tightly confines neutral atoms in three dimensions. It has a number of novel features compared to existing atom chip traps [18]. It does not require using fields generated by macroscopic coils. The trapped atoms are also not positioned directly above a wire as in the so-called “Z” and “U” traps. This opens up the possibility of studying the interaction of the atoms with the surface. Moreover, the distance of the atom cloud above the atom chip can be precisely varied using a bias magnetic field. Finally, the microtrap uses a relatively simple wire configuration that can be the unit cell of a one- or two-dimensional microtrap array.

The paper is organized as follows. First, the microtrap is described. Next, the apparatus and procedure used to load atoms from a magneto-optical trap (MOT) into a quadrupole trap, which was transported to the atom chip where atoms were loaded into the microtrap array, are discussed. Finally, experimental results and conclusions are presented. This includes a discussion of how the trap dimensions can be reduced by more than an order of magnitude, which is of

interest for creating an array of micrometer-sized neutral atom traps on a single atom chip.

2. DOUBLE-LOOP MICROTRAP

A schematic diagram of the array of three double-loop microtraps is shown in Fig. 1. Each microtrap consists of two circular wire loops having radii r_1 and $r_2 = \alpha r_1$ carrying oppositely oriented currents I . The centers of neighboring traps are spaced a distance $5r_1$ apart. The magnetic field along the z direction perpendicular to the microtrap surface is zero at position

$$z_0 = \frac{\alpha^{2/3}}{\sqrt{1 + \alpha^{2/3}}} r_1. \quad (1)$$

This current configuration generates a three-dimensional trap, as shown in Figs. 1(c) and 1(d), which shows the trap potential along the x and y directions evaluated for $z = z_0$. The value of $\alpha = 2.195$ was chosen to maximize the force along the z axis toward the trap minimum position. The computed potentials displayed in Fig. 1 take into account the effect of the finite straight-wire sections connecting adjacent loops. The currents in these straight-wire segments were found to have a negligible effect on the trap potential.

Figure 1(b) shows the trap is asymmetric along the z direction. A deeper and symmetric trap is obtained by adding a uniform bias field in the z direction, B_{bias} . The bias field also shifts the trap center closer to the chip surface. Figure 2 shows the maximum trap-depth dependence on the bias field, which was computed by multiplying the trapping field strength by the Bohr magneton and dividing by Boltzmann's constant. The maximum trap depth for the case of an isolated single microtrap occurs at a field of $B_{\text{bias}} = 1.43B_0$, where $B_0 = (\mu_0/4\pi)(I/r_1)$ and μ_0 is the magnetic permeability of vacuum. The addition of neighboring traps slightly affects the trap potential. The nearest neighboring traps increase the maximum trap depth, which occurs at a bias field of $B_{\text{bias}} = 1.65B_0$, as shown in Fig. 2. However, the effect of the

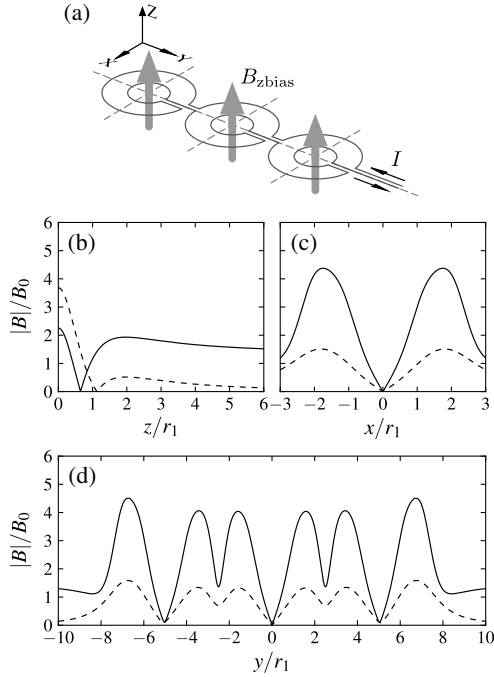


Fig. 1. Diagram of a linear array of three double-loop microtraps. Each of the three traps shown in (a) consists of two concentric loops of radii r_1 and $r_2 = 2.19r_1$. The trap centers are located a distance $5r_1$ apart. The trap potential along the z direction is shown in (b), where the z axis is defined as perpendicular to the chip and passes through the center of the middle microtrap. The trap potential along the x direction for the middle trap is shown in (c) and in the y direction is given in (d). The dashed curves were computed using a zero bias field, while the solid curve was found using $B_{\text{zbias}} = 1.43B_0$. The results shown in (c) and (d) were computed at the position $z = z_0$ along the z axis.

next nearest neighboring traps was negligible when one considered a linear array of five traps. Hence, the individual microtraps of a large array will have nearly identical potentials.

The trap potential shown in Fig. 1 has a zero minimum magnetic field. This can result in loss of atoms due to Majorana transitions, which is disadvantageous for evaporative cooling. This situation is avoided with a more complex wire configuration to generate a trap having a nonzero field minimum [1]. For example, in the case of the microtrap described in this paper, one can use two additional straight microwires positioned on either side of the microtrap array [19].

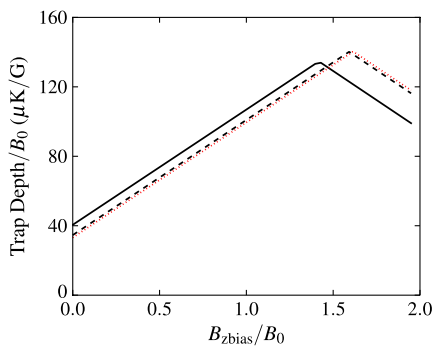


Fig. 2. (Color online) Trap-depth dependence on bias field B_{zbias} . The trap depth is shown for a single microtrap by the solid black curve. The trap depth of the middle microtrap is shown for a linear array of three microtraps (dashed curve) and five microtraps (dotted red curve).

This paper reports on the demonstration of a double-loop microtrap for the case of an inner microwire loop radius $r_1 = 300 \mu\text{m}$. A smaller value of r_1 was not used to facilitate a first demonstration of transferring atoms from a quadrupole trap into the microtrap array and readily image the resulting trapped atom clouds. The trap was loaded using ultracold ^{87}Rb atoms optically pumped to the $|F = 2, m_F = 2\rangle$ ground-state hyperfine level where F denotes the hyperfine level and m_F is its azimuthal component. For a 1 A trap current, $B_0 = 3.33$ Gauss and the trap has a depth of $115 \mu\text{K}$. This increased to $467 \mu\text{K}$ with the addition of a 5.5 Gauss z -bias field.

3. APPARATUS AND PROCEDURE

The apparatus is illustrated in Fig. 3. The atom chip, fabricated by Cold Quanta, had dimensions of 2 by 3 cm. The chip consisted of a 0.4 mm thick silicon dioxide substrate onto which a 10 μm thick copper layer was deposited. The chip contained three microtraps, as shown in Fig. 1. The microtrap wire pattern was created by etching 10 μm wide electrical insulating gaps in the mirror-quality copper layer on either side of the 50 μm wide wires. The microwires extended to two corners of the atom chip, where they were connected via wires to a power supply. The resistance of the microcircuit was measured to be less than 1Ω , in agreement with calculation. The atom chip was mechanically clamped onto a copper mounting block to facilitate heat dissipation. This block in turn was supported by a vacuum flange encapsulated by a borosilicate glass cell, which provided excellent optical access. The glass cell was antireflection coated for 780 nm. The vacuum system was initially pumped down using a turbo molecular pump. A 150 liter/s ion pump maintained a pressure of approximately 2×10^{-9} torr during the experiment.

The glass cell was surrounded by three pairs of coils, centered about a point 1.7 cm below the atom chip surface, that generated magnetic fields along the x and y directions. One pair of these coils, connected in the anti-Helmholtz configuration, generated a field gradient of up to 100 Gauss/cm along the axial direction x , required for the quadrupole trap. The coil pair generating the field in the y direction varied the position of the quadrupole trap facilitating its alignment with the microtrap. The third pair of coils generated a field of a few Gauss in the x direction that was used when optically pumping atoms into the $|F = 2, m_F = 2\rangle$ ground-state level. A single fourth coil having dimensions of 10 by 10 cm was positioned 2.3 cm above the atom chip surface as shown in Fig. 3. It generated a so-called B_{zshift} field in the vertical direction as high as 75 Gauss at the atom chip surface. This field was used to shift the quadrupole trap toward the microtrap, as will be discussed in the next section. The same coil also generated the microtrap bias field B_{zbias} . The magnitude of B_{zbias} at the centers of the three microtraps differed by less than three parts in 10^4 . All coils were connected to power supplies whose currents could be rapidly switched off using a LabVIEW program that had a timing resolution of 0.1 ms.

The original intent of the experiment was to load the microtrap with laser-cooled rubidium atoms generated by a mirror MOT using the copper surface of the atom chip as a mirror [18]. This succeeded, but the reflectivity of the copper decreased over time due to deposition of rubidium on the surface and oxidation resulting from an imperfect vacuum.

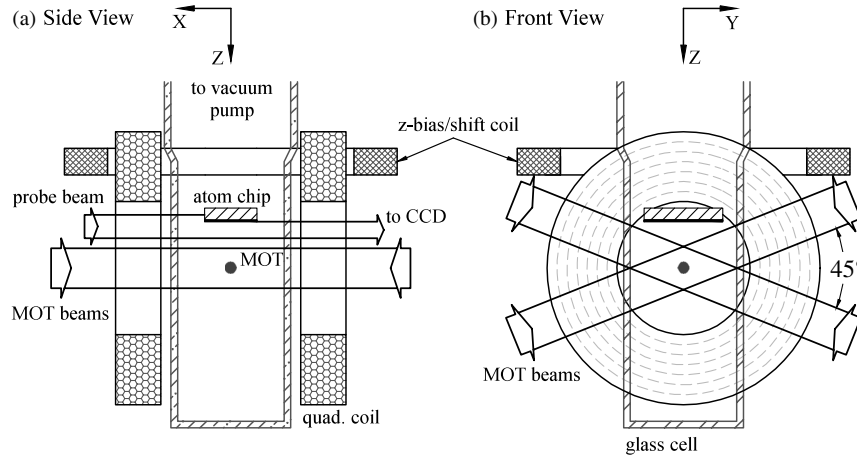


Fig. 3. Apparatus. The laser beams used to generate the MOT 1.7 cm below the atom chip surface are shown along with the probe beam used to image the atoms. See the text for a detailed description.

Hence, atoms were first laser cooled using a MOT created using three pairs of counter-propagating laser beams located below the atom chip surface. All results reported in this paper were obtained using this latter arrangement.

Atoms were loaded into a MOT from the background ^{87}Rb vapor, which was maintained by sending a current through a rubidium dispenser. The laser systems used in this experiment have been described in detail elsewhere [9,20]. The MOT laser beams in the vertical plane were retroreflected and intersected at a 45° angle as shown in Fig. 3, instead of at 90° to position the MOT atom cloud closer to the atom chip surface. The trap laser intensity for the MOT was about 3 mW/cm² with a beam diameter of about 18 mm for each laser beam. During the MOT loading, the trap laser was red detuned 2.4Γ , where $\Gamma/2\pi = 6.1$ MHz, from the $F = 2 \rightarrow F' = 3$ cycling transition of the D2 line where F and F' denote the hyperfine levels of the lower and excited states, respectively. A 4 mW repump laser beam, resonant with the $F = 1 \rightarrow F' = 2$ transition of the D2 line, overlapped with the trap laser beams, preventing atoms from accumulating in the $F = 1$ ground-state hyperfine level. The magnetic-field gradient for the MOT loading was 14 Gauss/cm along the x direction. Typically, 4×10^7 atoms were loaded into the MOT in 4 s. The atoms were further cooled by first compressing the MOT for 50 ms by ramping up the magnetic field gradient to 35 Gauss/cm and further shifting the trap laser red detuning to 5Γ . This was followed by a polarization gradient cooling (PGC) phase lasting 8 ms. All magnetic fields were turned off at the beginning of the PGC phase, and the trap laser detuning jumped to 10Γ . The resulting cloud of 4×10^7 atoms had a peak density of 1.5×10^{10} atoms/cm³ and a temperature of 40 μK , as determined using the time-of-flight method [21].

Following the PGC phase, the atoms were optically pumped for 1 ms using part of the cooling laser frequency shifted into resonance with the $F = 2 \rightarrow F' = 2$ transition of the D2 line. This facilitated the transfer of more than 90% of the MOT atoms into the quadrupole trap. The temporal sequence used to transfer atoms from the quadrupole trap into the microtrap is shown in Fig. 4, beginning from the time the quadrupole trap current I_{quad} was turned on. Atoms were contained in the quadrupole trap for 100 ms. For the next 200 ms, the z -shift field, $B_{z\text{shift}}$, was ramped up linearly to shift the quadrupole

trapped atom cloud to the atom chip surface [8,22]. The field gradient in the x direction of the quadrupole trap was reduced from 100 Gauss/cm by 10% when the trap was shifted close to the atom chip surface. Simultaneously, a magnetic field of a few Gauss was applied in the y direction, $B_{y\text{shift}}$, to align the quadrupole trap center with the atom chip microtrap. This alignment was checked by directing the probe laser beam vertically through the translated quadrupole trapped atom cloud and reflecting it off the atom chip surface. The CCD image showed whether the atom cloud overlapped with the microtrap. The efficiency of the atom transport from the original quadrupole trap to the atom chip surface was examined by moving atoms up to the chip surface and then back to the original quadrupole trap position. No measurable loss of atoms was observed. However, the atom cloud in the quadrupole trap, shifted near the atom trap, was elongated along the z direction. This reduced the atom density to 5×10^9 atoms/cm³. The atom temperature was measured to be 100 μK .

The transfer of atoms from the quadrupole trap to the microtrap occurred during a variable loading time interval. Simultaneous with the reduction of the quadrupole trap current, the magnetic field in the z direction was ramped down from $B_{z\text{shift}}$ to $B_{z\text{bias}}$ and the field in the y direction, $B_{y\text{shift}}$, was reduced to zero, while the chip current increased from 0 to 2.6 A. No increase in background pressure associated with chip heating of the microwires was observed.

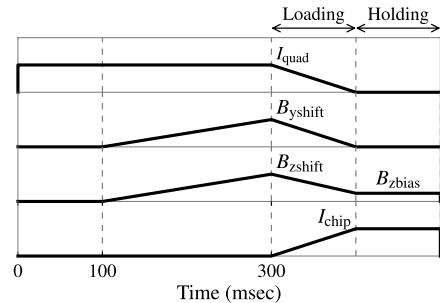


Fig. 4. Timing sequence of magnetic-field currents used to transfer atoms from the quadrupole trap into the microtraps. See text for a detailed description.

Atoms remained in the microtrap for a holding time, after which they were imaged by the probe laser.

The atom cloud in either the MOT or the microtrap was monitored by measuring the absorption of a probe laser that traversed the atom cloud using a CCD camera (Santa Barbara ST-10XME). It consisted of 2184×1472 pixels, each having a size of $(6.8 \mu\text{m})^2$. The probe laser was locked to the $F = 2 \rightarrow F' = 3$ transition of the D2 line. The probe laser beam passed through an acousto-optic modulator and a computer-controlled fast shutter that produced a $50 \mu\text{s}$ probe laser pulse having an intensity of $100 \mu\text{W}/\text{cm}^2$. The resulting two-dimensional spatial distribution of the cold atoms imaged on the CCD enabled the determination of the number of trapped atoms [20].

Each CCD image contained an interference fringe background that varied from one image to another. This was caused by vibrations of optical elements and fluctuations in air temperature or pressure [23]. This background was removed using the procedure developed by Ockeloen *et al.* [24]. Each day, 80 background images were taken with no trapped atoms present. The image of an atom cloud was processed by first considering only the portion of the image where the atom cloud was absent. A software program found the linear combination of background images best matching the interference pattern. This result was subtracted from the entire image.

4. RESULTS

Figure 5 shows a typical absorption image of the atom clouds trapped in the middle and left microtraps containing a total of 2×10^5 cold atoms. The trap was created using values of $B_{zshift} = 64$ Gauss, $B_{zbias} = 13$ Gauss, and a chip current of 2.6 A. No atoms were loaded into the rightmost microtrap because the quadrupole trap was located between the left two microtraps and no shifting field B_{yshift} was used. The atom cloud was probed 0.6 ms after the microtrap was turned off. The microtrap atom cloud was analyzed by fitting the

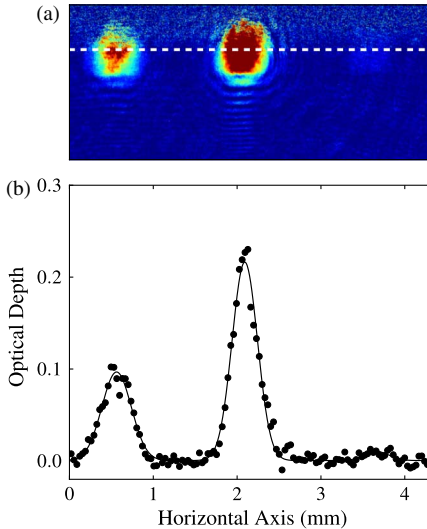


Fig. 5. (Color online) Absorption image of the center and left microtraps. Very few atoms were loaded into the right microtrap, as is discussed in the text. The profile of the atom cloud along the horizontal dashed line shown in (a) is given in (b). Each point represents an average of five pixels of data. The solid curve fitting each microtrapped atom cloud is a Gaussian function fitted to the data as described in the text.

absorption profile in the horizontal y direction to a Gaussian function given by

$$f(y) = Ae^{-\frac{(y-y_0)^2}{2\sigma^2}}, \quad (2)$$

where y_0 is the center position of the atom cloud and σ is the radius. The value for the middle trap cloud radius was found to be $150 \mu\text{m}$.

The number of atoms transferred from the quadrupole trap to the microtrap was comparable to the density of atoms in the quadrupole trap times the observed microtrap volume. A larger number of atoms could be loaded into a single microtrap using a quadrupole trap having a larger field gradient. However, this would have reduced the number of atoms loaded into adjacent microtraps of the linear array.

The dependence of the number of atoms in the middle microtrap on the shifting magnetic field, B_{zshift} , is shown in Fig. 6. At low fields, not many atoms were loaded into the microtrap because the quadrupole trap was not shifted upward sufficiently. At high fields, the atoms collided with the atom chip surface and were lost. The optimum number of atoms was transferred using a magnetic field of 63 ± 2 Gauss.

The dependence of the number of atoms in the middle microtrap as a function of the loading time is shown in Fig. 7. The data were modeled using

$$\frac{dN}{dt} = Re^{-t/\tau} - \alpha N, \quad (3)$$

where the first term describes loading N atoms into the microtrap at a rate R with a time constant τ during a time t [25]. The second term takes into account the loss of atoms during trap loading. An additional loss term due to collisions between cold microtrapped atoms was not considered because of the relatively low density ($\sim 10^{10}/\text{cm}^3$) of the microtrapped atom cloud. The best fit of Eq. (5) to the data gave values of $R = 1.26 \times 10^8 \text{ s}^{-1}$, $\tau = 75 \text{ ms}$, and $\alpha = 89 \text{ s}^{-1}$.

The effect of the bias magnetic field B_{zbias} on the middle microtrap is described in Fig. 8. Several thousand atoms were trapped without any bias field. This number is small because the trap depth is only 1/4 the maximum trap depth obtained using a bias field of $1.65B_0 = 14$ Gauss, as predicted by Fig. 2. This agreed closely with the observed field that maximized the number of microtrapped atoms. Figure 8 also shows how B_{zbias} shifted the microtrap atom cloud position toward the atom chip. These data agreed closely with the predicted location of the trap minima position. The dashed curve was found

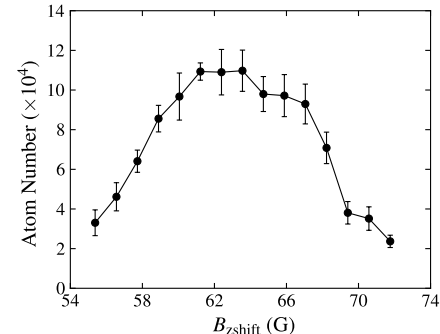


Fig. 6. Dependence of number of atoms in the middle microtrap on B_{zshift} .

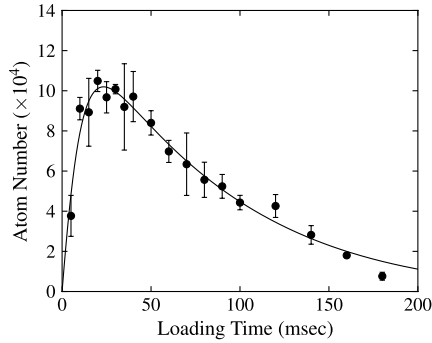


Fig. 7. Dependence of number of atoms in the middle microtrap on loading time. The solid curve is fit to the data using Eq. (5), as discussed in the text.

from the computed potentials shown in Fig. 1 and contained one adjustable parameter that specified the position of the atom chip surface. This parameter was chosen so the predicted curve best matched the observed data. The chip surface was not sharply defined in the CCD image because of diffraction of the probe laser beam. The probe laser direction was also not precisely parallel to the atom chip surface, resulting in a blurring of the exact surface position. This effect was also responsible for the relatively larger error bars for the data taken at the higher magnetic fields when the atom cloud was closest to the chip.

The temporal dependence of the number of atoms in the middle microtrap was examined by varying the trap holding time. The data were very well fitted to an exponential function having a lifetime of 336 ± 16 ms. This lifetime was limited by collisions with background gas atoms.

The temperature of the atoms in the microtrap was estimated in two different ways. First, images such as shown in Fig. 5 were taken using a current of 2.6 A, which corresponded to a trap depth of more than 1 mK. Smaller numbers of trapped atoms were observed using currents as low as 1 A. This indicated a temperature of a few hundred μK . The temperature was also determined from the size of the atom cloud in the microtrap. For simplicity, a one-dimensional model was considered. Figure 1 shows the microtrap potential near the trap center was well approximated by a linear function

$$U(y) = g_F m_F \mu_B B' y. \quad (4)$$

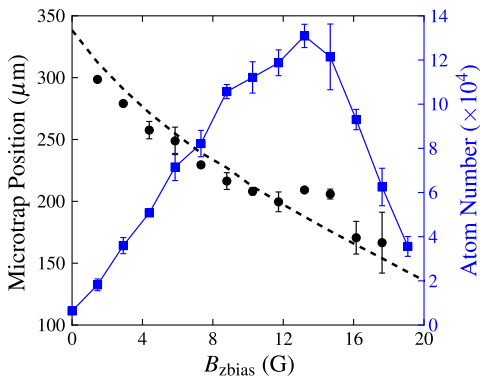


Fig. 8. (Color online) Effect of bias magnetic field on number of atoms in the middle microtrap and the center of its position. The dashed curve is the calculated trap position.

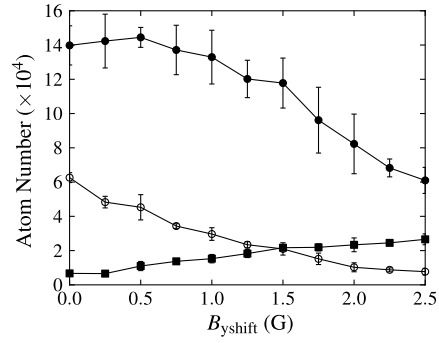


Fig. 9. Microtrap atom populations in left microtrap (open circles), middle microtrap (filled black circles), and right microtrap (filled black squares) as a function of $B_{y\text{shift}}$.

Here g_F is the Landé g factor, μ_B is the Bohr magneton, y is the position relative to the trap minimum, and B' is the field gradient along the y direction. Although the atom distribution in a linear trap is not Gaussian, this distribution can be used to estimate the atom cloud temperature. The average potential experienced by the atoms in the trap was found by integrating this potential over the observed distribution of atoms given by Eq. (4). Equating the average kinetic energy $(1/2)k_B T$, where k_B is Boltzmann's constant, to half of the potential energy as shown for a linear potential by the Virial theorem, gives the following expression for the atom temperature:

$$T = \sqrt{\frac{2g_F m_F \mu_B B' \sigma}{\pi k_B}}. \quad (5)$$

Substituting the observed atom cloud size in the horizontal direction gave a temperature of approximately 400 μK . The higher atom temperature in the microtrap compared to the quadrupole trap can be expected due to the so-called modal mismatch of the two trap potentials [2].

The distribution of atoms loaded into the linear array of three microtraps could be controlled using the magnetic field in the y direction, $B_{y\text{shift}}$, as is shown in Fig. 9. This field shifted the location of the quadrupole trap relative to the microtraps. The relative microtrap populations were varied using fields up to 2.5 Gauss, which was limited by the available power supply.

5. CONCLUSIONS

This experiment demonstrated a three-dimensional magnetic microtrap consisting of two concentric double loops whose size is characterized by the inner loop radius r_1 . More than 2×10^5 ^{87}Rb atoms were loaded into a linear array of three microtraps, each having a depth exceeding 1 mK. The atoms remained trapped for several hundred milliseconds. This undoubtedly could be increased if the background pressure was reduced to $< 10^{-10}$ torr pressure as is commonly achieved in BEC experiments. Atoms were loaded in a straightforward manner using a MOT and transported to the atom chip surface using a quadrupole trap. A bias field perpendicular to the microwire circuit increased the trap depth and controlled the position of the atom cloud relative to the atom chip surface. The coil generating this field could in the future be generated by a current loop mounted on the atom chip surrounding the microtraps. This would simplify the alignment of the fields necessary to steer atoms from the quadrupole trap into the

microtrap. The relative populations of the microtraps could be adjusted by a field oriented along the array direction.

A reduction of the microtrap size by more than an order of magnitude would be of particular interest for studying interactions between atom clouds spaced apart a distance comparable to the de Broglie wavelength. If the inner loop radius $r_1 = 10 \mu\text{m}$, the distance separating our present three traps would consist of a linear array of more than 50 microtraps. A corresponding two-dimensional array would have hundreds of microtrap elements. One could expect similar numbers of atoms to be loaded into neighboring microtraps from the quadrupole trap, although the number of atoms in each microtrap would be smaller than in the present experiment. The atom clouds could then be imaged using more sensitive techniques such as those used to study single trapped atoms [24,26]. The microtrap depth is proportional to the ratio of the current divided by the inner loop radius. Hence, the smaller trap would achieve the same depth using a factor of 10 less current. This in turn would permit a reduction of the micro-wire cross section, which is important as heat dissipation, which scales as the square of the current, is an important consideration for nonsuperconducting atom chips. The smaller traps would have a variable trap minimum position a distance of micrometers from the chip surface, which would be important for surface sensing experiments including studies of the Casimir Polder interaction [27,28]. Furthermore, the micro-wires only perturb a small portion of the surface, and this could be eliminated if the microwires were embedded in the chip. Hence, microtrap arrays open up interesting possible experiments in the studies of surface sensing and controlling the interactions between ultracold atoms.

ACKNOWLEDGMENTS

The authors thank I. DeSouza for technical assistance. Financial support from the Canadian Natural Science and Engineering Research Council is gratefully appreciated.

REFERENCES

1. J. D. Weinstein and K. G. Libbrecht, "Microscopic magnetic traps for neutral atoms," *Phys. Rev. A* **52**, 4004–4009 (1995).
2. R. Folman, P. Krager, J. Schmiedmayer, J. Denschlag, and C. Henkel, "Microscopic atom optics: from wires to an atom chip," *Adv. At. Mol. Opt. Phys.* **48**, 263–356 (2002).
3. J. Fortagh and C. Zimmerman, "Magnetic microtraps for ultracold atoms," *Rev. Mod. Phys.* **79**, 235–289 (2007).
4. W. Hansel, P. Hommelhoff, T. W. Hänsch, and J. Reichel, "Bose Einstein condensation on a microelectronic chip," *Nature* **413**, 498–501 (2001).
5. H. Ott, J. Fortagh, G. Schlötterbeck, A. Grossmann, and C. Zimmerman, "Bose Einstein condensation in a surface microtrap," *Phys. Rev. Lett.* **87**, 230401 (2001).
6. M. Horikoshi and K. Nakagawa, "Atom chip based fast production of a Bose Einstein condensate," *Appl. Phys. B* **82**, 363–366 (2006).
7. D. M. Farkas, K. M. Hudek, E. A. Salim, S. R. Segal, M. B. Squires, and D. Z. Anderson, "A compact, transportable, microchip based system for high repetition rate production of Bose Einstein condensates," *Appl. Phys. Lett.* **96**, 093102 (2010).
8. S. Aubin, S. Myrskog, M. H. T. Extavour, L. J. LeBlanc, D. McKay, A. Stummer, and J. H. Thywissen, "Rapid sympathetic cooling to fermi degeneracy on a chip," *Nat. Phys.* **2**, 384–387 (2006).
9. B. Lu and W. A. van Wijngaarden, "Bose Einstein condensation in a QUIC trap," *Can. J. Phys.* **82**, 81–102 (2004).
10. Y. Lin, I. Teper, C. Chin, and V. Vuletic, "Impact of the Casimir Polder potential and Johnson noise on Bose Einstein condensate stability near surfaces," *Phys. Rev. Lett.* **92**, 050404 (2004).
11. M. Gierling, P. Schneeweiss, G. Visanescu, P. Federsel, M. Haffner, D. P. Kern, T. E. Judd, A. Gunther, and J. Fortagh, "Cold atom scanning probe microscopy," *Nat. Nanotechnol.* **6**, 446–451 (2011).
12. Y. Wang, D. Z. Anderson, V. M. Bright, E. A. Cornell, Q. Diot, T. Kishimoto, M. Prentiss, R. A. Saravanan, S. R. Segal, and S. Wu, "Atom Michelson interferometer on a chip using a Bose Einstein condensate," *Phys. Rev. Lett.* **94**, 090405 (2005).
13. S. Kraft, A. Günther, P. Wicke, B. Kasch, C. Zimmerman, and J. Fortagh, "Atom-optical elements on microchips," *Eur. Phys. J. D* **35**, 119–123 (2005).
14. Y. Colombe, T. Steinmetz, G. Dubois, F. Linke, D. Hunger, and J. Reichel, "Strong atom field coupling for Bose Einstein condensates in an optical cavity on a chip," *Nature* **450**, 272–276 (2007).
15. G. Birk and J. Fortagh, "Microtraps for quantum information processing and precision force sensing," *Lasers Photon. Rev.* **1**, 12–23 (2007).
16. T. Calcaro, E. A. Hinds, D. Jaksch, J. Schmiedmayer, J. I. Cirac, and P. Zoller, "Quantum gates with neutral atoms: controlling collisional interactions in time dependent traps," *Phys. Rev. A* **61**, 22304 (2000).
17. P. Treutlein, T. W. Hänsch, J. Reichel, A. Negretti, M. A. Cirone, and T. Calcaro, "Microwave potentials and optimal control for robust quantum gates on an atom chip," *Phys. Rev. A* **74**, 22312 (2006).
18. J. Reichel, "Microchip traps and Bose Einstein condensation," *Appl. Phys. B* **74**, 469–487 (2002).
19. W. A. van Wijngaarden, "A second century of Einstein? Bose Einstein condensation and quantum information," *Can. J. Phys.* **83**, 671685 (2005).
20. B. E. Schultz, H. Ming, G. A. Noble, and W. A. van Wijngaarden, "Measurement of the Rb D2 transition linewidth at ultralow temperature," *Eur. Phys. J. D* **48**, 171–176 (2008).
21. D. S. Weiss, E. Riis, Y. Shevy, P. J. Ungar, and S. Chu, "Optical molasses and multilevel atoms: experiment," *J. Opt. Soc. Am. B* **6**, 2072–2083 (1989).
22. M. Greiner, I. Bloch, T. W. Hänsch, and T. Esslinger, "Magnetic transport of trapped cold atoms over a large distance," *Phys. Rev. A* **63**, 031401 (2001).
23. D. A. Smith, S. Aigner, S. Hofferberth, M. Gring, M. Andersson, S. Wildermuth, P. Krüger, S. Schneider, T. Schumm, and J. Schmiedmayer, "Absorption imaging of ultracold atoms on atom chips," *Opt. Express* **19**, 8471–8485 (2011).
24. C. F. Ockeloen, A. F. Tauschinsky, R. J. C. Spreeuw, and S. Whitlock, "Detection of small atom numbers through image processing," *Phys. Rev. A* **82**, 061606 (2010).
25. H. Ming and W. A. van Wijngaarden, "Transfer of ultracold ^{87}Rb from a QUIC magnetic trap into a far off resonance optical trap," *Can. J. Phys.* **85**, 247–258 (2007).
26. I. Teper, Y. J. Lin, and V. Vuletic, "Resonator-aided single-atom detection on a microfabricated chip," *Phys. Rev. Lett.* **97**, 023002 (2006).
27. J. M. Obrecht, R. J. Wild, M. Antezza, L. P. Pitaevskii, S. Stringari, and E. A. Cornell, "Measurement of the temperature dependence of the Casimir Polder force," *Phys. Rev. Lett.* **98**, 063201 (2007).
28. H. Bender, P. W. Courteille, C. Marzok, C. Zimmerman, and S. Slama, "Direct measurement of intermediate range Casimir Polder potentials," *Phys. Rev. Lett.* **104**, 083201 (2010).